J Nanopart Res (2015) 17:219
DOI 10.1007/s11051-015-3031-4

RESEARCH PAPER

Influence of clay particles on Al_2O_3 and TiO_2 nanoparticles transport and retention through limestone porous media: measurements and mechanisms

Ali Esfandyari Bayat · Radzuan Junin · Rahmat Mohsin · Mehrdad Hokmabadi · Shahaboddin Shamshirband

Received: 31 January 2015 / Accepted: 7 May 2015 / Published online: 15 May 2015

Abstract Utilization of nanoparticles (NPs) for a broad range of applications has caused considerable quantities of these materials to be released into the environment. Issues of how and where the NPs are distributed into the subsurface aquatic environments are questions for those in environmental engineering. This study investigated the influence of three abundant clay minerals namely kaolinite, montmorillonite, and illite in the subsurface natural aquatic systems on the transport and retention of aluminum oxide (Al_2O_3, 40 nm) and titanium dioxide (TiO_2, 10–30 nm) NPs through saturated limestone porous media. The clay concentrations in porous media were set at 2 and 4 vol% of the holder capacity. Breakthrough curves in the columns outlets were measured using a UV–Vis spectrophotometer. It was found that the maximum NPs recoveries were obtained when there was no clay particle in the porous medium. On the other hand, increase in concentration of clay particles has resulted in the NPs recoveries being significantly declined. Due to fibrous structure of illite, it was found to be more effective for NPs retention in comparison to montmorillonite and kaolinite. Overall, the position of clay particles in the porous media pores and their morphologies were found to be two main reasons for increase of NPs retention in porous media.

Keywords Nanoparticle · Stability · Transport and retention · Clay particle · Environmental effects

A. E. Bayat (✉) · R. Junin · M. Hokmabadi
Department of Petroleum Engineering, Faculty of Petroleum and Renewable Energy Engineering, Universiti Teknologi Malaysia, UTM Skudai, 81310 Johor Bahru, Malaysia
e-mail: ali.esfandiari.bayat@gmail.com

R. Junin · R. Mohsin
UTM-MPRC Institute for Oil and Gas, N29A, Lengkuk Suria, Universiti Teknologi Malaysia, UTM Skudai, 81310 Johor Bahru, Malaysia

S. Shamshirband
Department of Computer System and Information Technology, Faculty of Computer System and Information Technology, University of Malaya, 50603 Kuala Lumpur, Malaysia

Introduction

Aluminum oxide (Al_2O_3) and titanium dioxide (TiO_2) are the two most common metal oxide nanoparticles (NPs) widely utilized in various industries including food processing, cosmetics, pigments, paints, electronics, and catalysts (Chen et al. 2011; Piccinno et al. 2012; Jiang et al. 2012). Therefore, considerable quantities of Al_2O_3 and TiO_2 NPs are released into the environment daily. Generally, NPs have the potential to be transported to the subsurface alluvial zones and they will reach and contaminate drinking groundwater resources because of their tiny dimensions (Chowdhury et al. 2011). The international agency for research on cancer (IARC) has classified Al_2O_3 and TiO_2 NPs as

carcinogenic to humans since the toxicity of these NPs is much greater than the bulk formulations with the same chemistry (Nel et al. 2006; Krewski et al. 2007; Scown et al. 2010). However, issues such as how and where the released NPs are distributed into the subsurface remain major challenges for environmental engineering (Handy and Shaw 2007; Darlington et al. 2009). In addition, the applications of Al_2O_3 and TiO_2 NPs as agents for enhanced oil recovery (EOR) purpose have been recently proven (Esfandyari Bayat et al. 2014a; Hendraningrat and Torsæter 2015). Use of these metal oxide NPs is a new task in petroleum engineering and needs to be tested and validated before they are applied on a fully pledged scale. NPs usage for EOR is also facing the same question of how these NPs are transported through hydrocarbon reservoirs. NPs can precipitate in hydrocarbon reservoir pores and consequently clog them during transport. Consequently, the permeability of reservoir is reduced resulting in a decline of hydrocarbon reservoir productivity. Thus, prior to the use of NPs for EOR implementation, the effects of the different parameters on the NPs transport need to be determined.

To date, great efforts have been carried out on the transport and retention of Al_2O_3 and TiO_2 under environmentally relevant conditions. For example, the effects of different physicochemical parameters such as size, concentration, and shape of NPs (Lecoanet et al. 2004; Darlington et al. 2009; Auffan et al. 2009; Jiang et al. 2009; Wang et al. 2013), NP surface coating (with surfactant, polymer and or NOM) (Phenarat et al. 2008; Godinez and Darnault 2011; Aiken et al. 2011), fluid velocity (Lecoanet et al. 2004; Chowdhury et al. 2011),and solution chemistry (i.e., ionic strength, pH, and ion type) (French et al. 2009; Ben-Moshe et al. 2010; Chen et al. 2011; Godinez and Darnault 2011; Esfandyari Bayat et al. 2014b) on the transport and retention of the mentioned NPs have been determined.

Presence of clay particles in porous media is another influential parameter on NPs transport (Schroth and Sposito 1997; Vasiliadou and Chrysikopoulos 2011; Syngouna and Chrysikopoulos 2013; Cai et al. 2014). Clay particles are the most abundant inorganic colloids in natural aquatic systems (Cai et al. 2014) and there are approximately thirty different types (Wilson et al. 2014). Kaolinite, montmorillonite, illite, and chlorite are the most common clay minerals which are ubiquitously found in the subsurface environment (Wilson et al. 2014). Other clay types are those composed of a mixture of these four clays (Jiang 2012). Clay particles have a high potential to interact with other (bio) colloids and could serve as carriers of colloids due to their surface charge heterogeneity (Schroth and Sposito 1997; Vasiliadou and Chrysikopoulos 2011; Syngouna and Chrysikopoulos 2013; Cai et al. 2014). Depending on the physicochemical conditions in the porous media, clay particles may facilitate or hinder the mobility of colloids in a study by Yang et al. (2012), they found that the presence of bentonite in suspensions significantly reduced the transport of bacteria in the quartz sand porous media while Abdel-Fattah et al. (2013) observed that the plutonium colloids transport was facilitated though subsurface soil by presence of smectite clay. Furthermore, Fang et al. (2009) evaluated TiO_2-NP transport through different soil types. They found that the mobility of TiO_2 was significantly reduced through soil columns especially in those porous media with higher concentrations of clay minerals. In contrast, Cai et al. (2014) found that the presence of suspended clay particles (i.e., bentonite and kaolinite) facilitated the mobility of TiO_2-NPs through quartz sand porous media.

Although each of the mentioned studies in the previous paragraph had worthy findings, it is difficult to find and allocate a general rule for the effects of clay particles since the obtained results are in contrast. Furthermore, how the presence of clay particles affects NPs transport is another question that needs to be studied. Thus, more studies are required to investigate the roles of clay particles on NPs transport. This study was designed to determine and compare the influence of three clay minerals namely kaolinite, illite, and montmorillonite in saturated limestone porous media on Al_2O_3 and TiO_2 NPs transport. The reason of the selection of limestone as porous medium was due to the fact that a significant portion of underground water resources are located in such rocks (Esfandyari Bayat et al. 2014b). In addition, another significance of the selection is due to the fact that limestones occupy approximately 40 % of hydrocarbon resources in the world (Salehi et al. 2008). To prove the transport tests results, field emission scanning electron microscopy (FESEM) and energy dispersive X-ray (EDX) analyses were utilized. Furthermore, classical Derjaguin–Landau–Verwey–Overbeek (DLVO) theory was applied to qualitatively assess and explain the reason(s) of the NPs deposition through porous media.

Methods and methodology

NPs suspensions preparation and characterization

Aluminum oxide (alpha-Al_2O_3, with nominal size of 40 nm, purity 99 %) and titanium dioxide (anatase-TiO_2, with nominal size of 10–30 nm, purity 99.5 %) nanopowders, received from SkySpring Nanomaterials, Inc., (Houston, TX), were utilized in this study. Transmission electron microscopy (TEM, Model JEM-2100/HR, JEOL, Acc.200.00 kV) and X-ray diffraction (XRD, model D5000, SIEMENS) analyses were firstly performed to recheck the NPs morphologies and compositions. Then, Al_2O_3 and TiO_2 NPs suspensions were prepared by adding 50 mg of the each nanopowder to 1 L of de-ionized water (DIW). DIW was selected as background solution in this study to avoid the effects of solution chemistry (e.g., pH and or ionic strength) on the NPs stability and transport. The NPs suspensions were agitated for 1 h using an orbital shaker at 220 rpm and ultrasonicated by an ultrasonic bath for a period of 1 h to obtain homogenous suspensions prior to each test. The pH values of Al_2O_3 and TiO_2 NPs suspensions were measured to be 6.5 ± 0.1 and 6.2 ± 0.1, respectively, using a digital pH meter (EUTECH Instruments, model pH700). To measure the stability of NPs against deposition in DIW, sedimentation tests were carried out (Godinez and Darnault, 2011). For this purpose, the amount of NPs deposition was recorded in each 5 min intervals over a 180 min time span with the use of time-resolved optical absorbance. The absorbance of the samples was measured using an ultraviolent visible (UV–Vis) spectrophotometer (Model 105, BUCK SCIENTIFIC., Inc.) over the wavelength range of 200–800 nm. Calibration was based on the maximum absorbance wavelength of 400 nm. The named experiments were repeated three times, and the presented data are the average of the obtained records.

The average ζ-potential value of the NPs in DIW was measured by a ZEECOM zeta potential analyzer instrument (Microtec Co., Ltd). The NPs suspensions were prepared, sonicated for 1 h, and shaken prior used for the ζ-potential measurements. The ζ-potential values were obtained by averaging three ζ-potential measurements for each NP suspension. Moreover, the radius of NP aggregates in DIW was measured using a DynaPro Titan Dynamic Light Scattering (DLS) probe from Wyatt Technology Corporation. The NPs suspensions were prepared as indicated for the ζ-potential measurements. DLS scattering analysis was performed three times (20 DLS reading per each run) for each NP suspension. The mean value of the measurements was applied to determine the radius of NPs aggregates. All these characterization techniques were conducted at room temperature (26 °C).

Porous media preparation and characterization

A limestone sample, collected from a surface outcrop in Ipoh-Malaysia, was utilized as the porous medium in this study. The sample of limestone was broken off into the smaller pieces, and then crushed to fine grains using a crusher machine (PULVERIZER Type from BICO, Inc.,). The limestone grains were sifted through 125 and 175 μm stainless steel sieves (USA Standard Testing Sieves, ATM Corp., New Berlin, WI) to achieve an average collector diameter (d_c) of 150 μm. Then, the limestone grains were pre-treated using a sequential water rinse, ultrasonication, and oven-drying procedure at 110 °C for 10 h to eliminate impurities. Moreover, kaolinite (size 20 μm and density 2.67 g/cm^3), illite (size 20 μm and density of 2.76 g/cm^3), and montmorillonite (size 40 μm and density of 2.68 g/cm^3) powders, received from SunClayTherapy, Inc. (Florida, US) and without further purification, were utilized as clay particles. To determine the exact morphologies of limestone grains and clay particles, scanning electron microscope (SEM, Philips XL40) and FESEM (HITACHI, SU8020) images were prepared from them before and after performing the transport experiments. Furthermore, EDX and XRD analyses were also carried out to determine the limestone and clay particles compositions. Besides that, the ζ-potential value of the named samples was measured using the method detailed by Tufenkj and Elimelech (2004).

A stainless steel tube with an inner diameter of 0.9 cm and a length of 33 cm was utilized as the porous medium holder. A 5 micron filter cloth was placed at both ends of the tube to prevent the grains migration during the transport tests. 30 gr of the cleaned limestone grains were averagely used in each experimental trial. Furthermore, kaolinite, montmorillonite, and illite powders in the range of 2 and 4 vol% of the holder capacity were also mixed to the limestone grains and then they were slowly loaded into the column. The column was wet packed uniformly using the method

explained by Chen et al. (2011). Once the column was packed, it was saturated with approximately ten pore volumes (PVs) of DIW in a vertical upward direction using a syringe pump (Model PSK-01; NIKKISO Co., Ltd) at a constant Darcy velocity of 4.66×10^{-3} cm/s (flow rate of 1 cm^3/min) to ensure a homogenous saturation of the pack. It should be noted that the flow direction was selected to be vertically upward to equilibrate the influent solution and enhance packing homogeneity (Godinez and Darnault, 2011). Finally, the porosity (φ) and permeability (k) of the packed column was measured according to the related ASTM standard methods.

Column transport test

After the column preparation, a pulse of each NP suspension (50 mg/L) with Darcy velocity of 4.66×10^{-3} cm/s was injected into the column for two PVs. Thereafter, DIW with the same Darcy velocity was injected into the column until no NP was observed in the outlet to check for mobilization of the trapped NPs in the porous medium. At the same time, the effluent samples were collected using a fraction collector (CF-2, Spectrum Chromatography, Houston, TX, USA) in 2 cm^3 sample sizes. The NPs concentration in the collected samples was measured using the UV–Vis spectrophotometer. Finally, the concentration of NPs dispersions entering the porous medium, C_O, and in the outlet, C, were applied to generate breakthrough curve of C/C_O as function of PVs passing through the porous medium. All transport experiments were repeated at least three times, and the presented data are the average of the obtained records. Moreover, the transport tests were performed at room temperature (26 °C).

DLVO theory

The NPs transport tests results were checked via classical DLVO theory. This theory was applied to qualitatively explain and compare the interaction between NP–NP and between NP–porous medium grain (collector) (Ben-Moshe et al. 2010; Chen et al. 2011; Esfandyari Bayat et al. 2015). For this aim, the total NP–NP and NP–collector interaction energies as the summation of van der Waals (VDW) and electrostatic double layer (EDL) interactions were calculated. For the calculation of the NP–NP interaction energy, it was assumed that NPs are spherical while for NP–collector interaction, it is assumed that the NP is spherical and collector is flat (Chen et al. 2011; Chowdhury et al. 2011; Esfandyari Bayat et al. 2014a, 2014b). The VDW attractive interaction energies for the NP–NP ($E_{VDW\text{-}NN}$) and NP–collector ($E_{VDW\text{-}NC}$) systems are computed as:

$$E_{VDW-NN} = -\frac{A_{131}}{6}\left[\frac{2a_p^2}{D(4a_p + D)} + \frac{2a_p^2}{(2a_p + D)^2} + \ln\left(\frac{D(4a_p + D)}{(2a_p + D)^2}\right)\right] \quad (1)$$

$$E_{VDW-NC} = -\frac{A_{132}a_p}{6D}\left[1 + \frac{14D}{\lambda}\right]^{-1}, \quad (2)$$

where A_{131} is Hamaker constant for NP–water–NP (for Al_2O_3 NP–NP 5.3×10^{-20} J; for TiO_2 NP–NP 6.0×10^{-20} J were utilized Petosa et al. 2010) and A_{132} is Hamaker constant for NP–water–collector (for Al_2O_3 NP-limestone 3.67×10^{-20} J and for TiO_2 NP-limestone 1.4×10^{-20} J were utilized Petosa et al. 2010), a_p is the radii of NP aggregates, D is the separation distance, and λ is the characteristic wavelength of interaction that is assumed 100 nm.

In addition, the EDL interaction energies for the NP–NP ($E_{EDL\text{-}NN}$) and NP–collector ($E_{EDL\text{-}NC}$) systems are calculated as:

$$E_{EDL-NN} = \frac{64\pi\varepsilon_0\varepsilon_r k_B^2 T^2 a_p^2}{e^2 z^2} \times \tanh^2\left(\frac{ze\Psi_p}{4k_B T}\right) \times \frac{\exp(-\kappa D)}{2a + D} \quad (3)$$

$$E_{EDL-NC} = \pi\varepsilon_0\varepsilon_r a_p\left(\xi_p^2 + \xi_c^2\right)\left\{\frac{2}{(\xi_p^2 + \xi_c^2)}\ln\left(\frac{1 + \exp(-\kappa D)}{1 - \exp(-\kappa D)}\right) + \ln(1 - \exp(-2\kappa D))\right\}, \quad (4)$$

where k_B is the Boltzmann constant (1.3805×10^{-23} J/°K), T is the absolute temperature of the system (298.15°K), ε_0 is the permittivity of free space (8.85×10^{-12} C/V/m), ε_r is the relative dielectric constant of water (78.5), Ψ_p is the reduced potential ($\Psi_p = \frac{ze\xi}{k_B T}$) of NP ξ_p, and ξ_c are the electrical

potentials of the NP aggregate and the collector, e is the electron charge (1.602×10^{-19} C), z is the valence of ion in bulk solution, and κ is the Debye–Hückel reciprocal length and is calculated as:

$$\kappa = \left(\frac{2000e^2 N_A I}{\varepsilon_0 \varepsilon_r k_B T}\right)^{0.5}, \quad (5)$$

where N_A is the Avogadro's number (6.022×10^{23}) and I is the ionic strength (for DIW it is assumed $10^{-5.5}$ M).

Results and discussion

NPs characterizations results

According to TEM images, the morphology of Al_2O_3 and TiO_2 nanopowders appeared to be spherical (Fig. 1). The results of XRD analyses also confirmed that the composition of NPs is Al_2O_3-alpha and TiO_2-anatase as shown in Fig. 1. Furthermore, the average ζ-potential value of Al_2O_3 and TiO_2 NPs in the DIW was measured to be as +19.1 and +9.1 mV, respectively. Besides that, the size of Al_2O_3 and TiO_2 NP aggregates in DIW was measured to be 255 and 220 nm, respectively.

The sedimentation analysis results also depicted the stability of Al_2O_3-NPs suspension against deposition was 9 % greater than TiO_2 at 180th min (Fig. 2a). The interaction between particles is one of the factors which determines the NPs stabilities in a solution (Esfandyari Bayat et al. 2014b). For this aim, DLVO theory is applicable to qualitatively explain this interaction (Hotze et al. 2010). The interaction between two particles can be repulsion or attraction. The electrostatic double layer (EDL) is a force which drives particles apart while the van der Waals (VDW) force drives particles toward each other. The summation of these forces clarifies whether the net interaction between two particles is attractive or repulsive (Bian

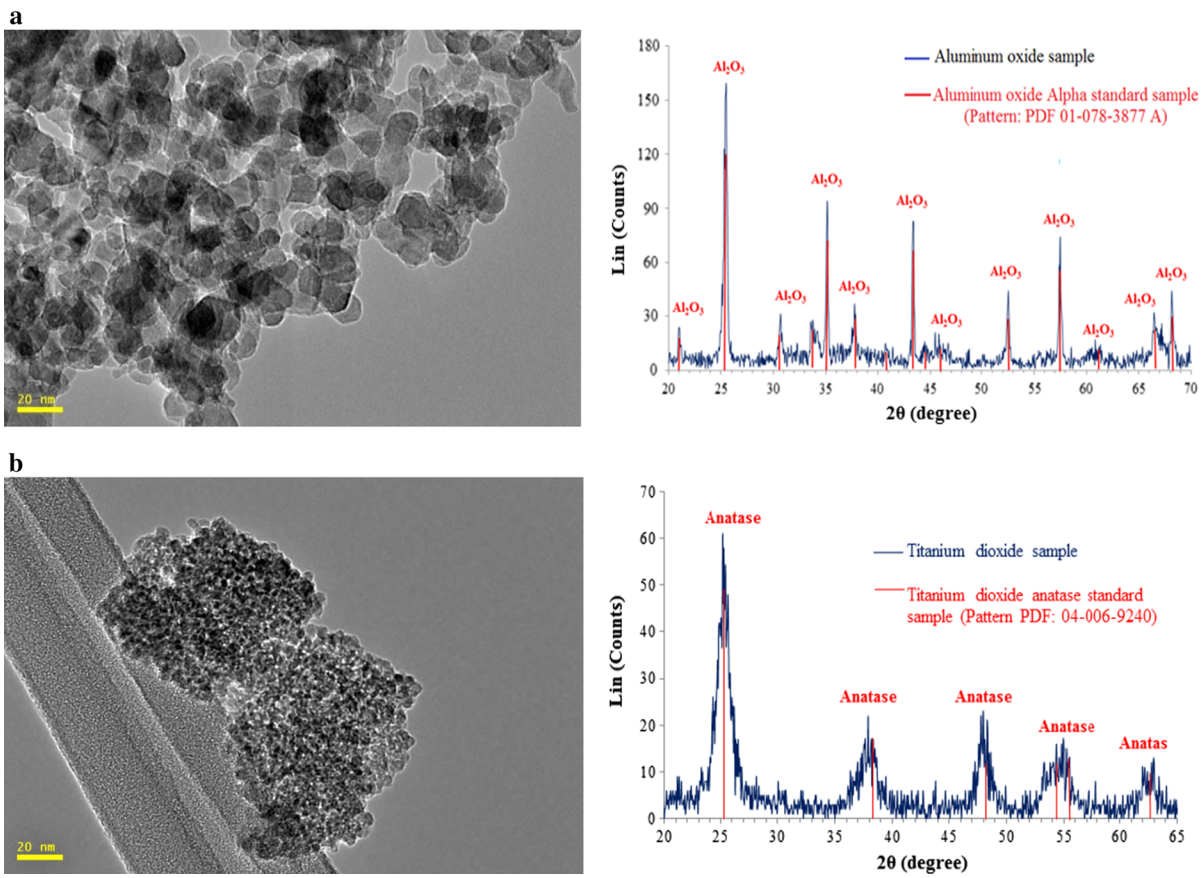

Fig. 1 TEM (*left*) and XRD (*right*) analyses results from the nanopowders **a** Al_2O_3-NPs, **b** TiO_2-NPs

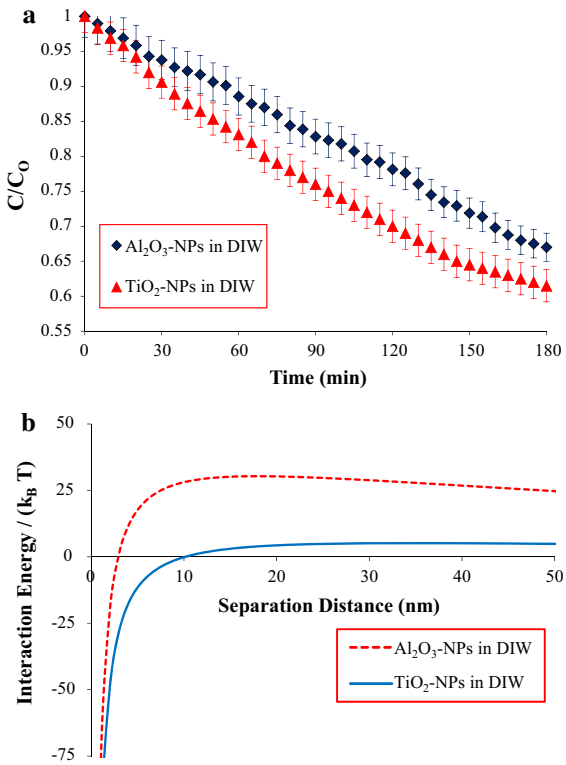

Fig. 2 **a** Sedimentation tests results, **b** NP–NP interaction energy profiles generated by DLVO theory

et al. 2011). High positive values of the total interaction energy imply that the EDL force is greater in magnitude and it is the dominant force (Esfandyari Bayat et al. 2015). The total interaction energy for NP–NP as a function of distance for the both Al_2O_3 and TiO_2 NPs were calculated and drawn. As shown in Fig. 2b, the EDL is dominant force among Al_2O_3 and also TiO_2 NPs. However, the interaction energy height for Al_2O_3-NPs is six times higher than TiO_2 which reveals higher repulsion force among Al_2O_3-NPs. Consequently, Al_2O_3-NPs suspension was more stable than TiO_2-NPs suspension. Therefore, DLVO theory supports our experimental results.

Al_2O_3 and TiO_2 NPs transport through limestone

First transport test was carried out by Al_2O_3-NPs suspension through the limestone porous medium. The Al_2O_3-NPs breakthrough curve is shown in Fig. 3a. The NPs received in the column effluent right after 1st PV of injection. The NPs concentration (C/C_O) value in the outlet remarkably increased to 0.104 until 15th PVs. Thereafter, the NPs recovery moderately decreased to 0 at 27.5th PVs. After this PV, Al_2O_3 was not observed in the effluent even after addition of extra ten PVs of DIW. The result demonstrated that 91.8 % of entered Al_2O_3-NPs was recovered from the column.

High Al_2O_3-NP recovery is attributed to its stability in DIW against deposition as well as the electric surface charge signs of Al_2O_3-NPs (+19.1 mV) and limestone grains (+33.1 mV) which are both positive. According to DLVO, the interaction energy height between Al_2O_3-NPs and limestone grains is quite high (+88) which reveals that a strong repulsion force between the NPs and grains (Fig. 4a). As a result, the Al_2O_3-NPs had low affinity to adsorb on the limestone grains surfaces. Moreover, 8.2 % of Al_2O_3-NPs remained in the porous medium that is attributed to the morphology of the limestone grains. The SEM images from limestone grains reveal that the grains surfaces are full of irregular dents and bumps (Fig. 5a). Therefore, there is a high possibility that the remained NPs became trap inside the porous medium.

The next transport test was performed for TiO_2-NPs. The NPs were received in the column outlet after injection of 1.2 PVs. The TiO_2-NPs breakthrough curve is shown in Fig. 3a. Accordingly, 72.2 % of the entered TiO_2-NPs into the column was collected. While the DLVO calculations demonstrate that the interaction between TiO_2-NPs and limestone grains is repulsive (Fig. 4a), 27.8 % of the NPs remained in the porous medium. To Figure out the reason(s) why the TiO_2-NPs recovery through the limestone porous media is lower than Al_2O_3, the results from these two transport tests should be compared. As discussed in the previous section, the sedimentation tests and DLVO theory results confirmed that the stability of TiO_2-NPs in DIW against deposition is lower than Al_2O_3 over time (Fig. 2). Yu et al. (2012) and Esfandyari Bayat et al. (2014b) declared that mobility of NPs through porous media is a function of their stabilities where lower stabilities lead to mobility reduction. Thus, the lower TiO_2-NPs stability as compared to the Al_2O_3 is one of the reasons for the lower TiO_2-NPs recovery. In addition, the calculated interaction energies between the NPs and limestone grains reveal that the interaction energy height between Al_2O_3-NPs and limestone grains is 4.6-fold higher than TiO_2-NPs and limestone grains (Fig. 4a). Thus, higher repulsion force between Al_2O_3-NPs and

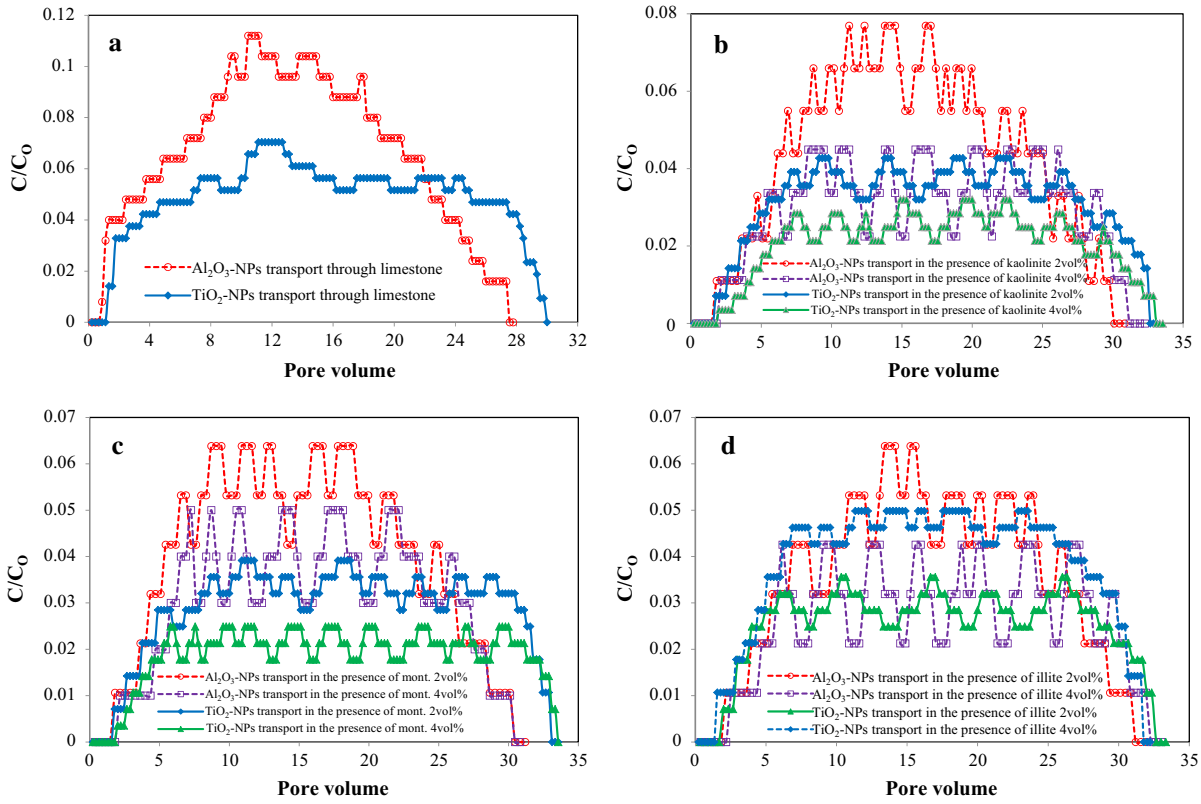

Fig. 3 NPs breakthrough curves transported through various porous media, **a** without presence of clay particles, **b** in the presence of kaolinite particles, **c** in the presence of montmorillonite particles, **d** in the presence of illite particles

limestone grains as compared to TiO_2-NPs can be another reason for easier Al_2O_3-NPs transport through the limestone porous medium.

Al_2O_3 and TiO_2 NPs transport in the presence of kaolinite

As mentioned in the methodology, characterization tests including FESEM, EDX, and ζ-potential were performed on the clay particles prior to the column tests. As shown in Fig. 6a, the morphology of kaolinite particles is booklet shape and the elements including O, Si, Al, K, Ca, Cr, and Fe were detected in the kaolinite sample. Besides that, the surface charge of kaolinite sample was measured to be $+6.1 \pm 0.5$ mV.

After the columns were packed, the porosity and permeability of porous media were firstly measured (Table 1). Then, Al_2O_3 and TiO_2 NPs transport tests through these porous media were carried out. The profiles of Al_2O_3 and TiO_2 NPs breakthrough curves in the presence of kaolinite are shown in Fig. 3b. Based on the obtained results, increasing kaolinite concentrations from 0 to 4 vol% resulted in the noticeable declining of Al_2O_3-NPs recoveries from 91.8 to 46.5 % as well as reduction of TiO_2-NPs recoveries from 72.2 to 34.3 %. Furthermore, it was observed that the NPs breakthrough time and period of experiment extended with the increase in kaolinite concentration. Reduction in the value of maximum NPs concentrations (C/C_O max) in the outlet and increasing in the number of fluctuations in the breakthrough curves were also another observed parameters during the tests (Fig. 3b). The details of NPs transport tests are also demonstrated in Table 1.

Few recent studies also found that the presence of kaolinite particles in porous media significantly decreased TiO_2 and SiO_2 NPs as well as microbe transport through sandy porous media (Fang et al. 2009; Caldelas 2010; Vasiliadou and Chrysikopoulos

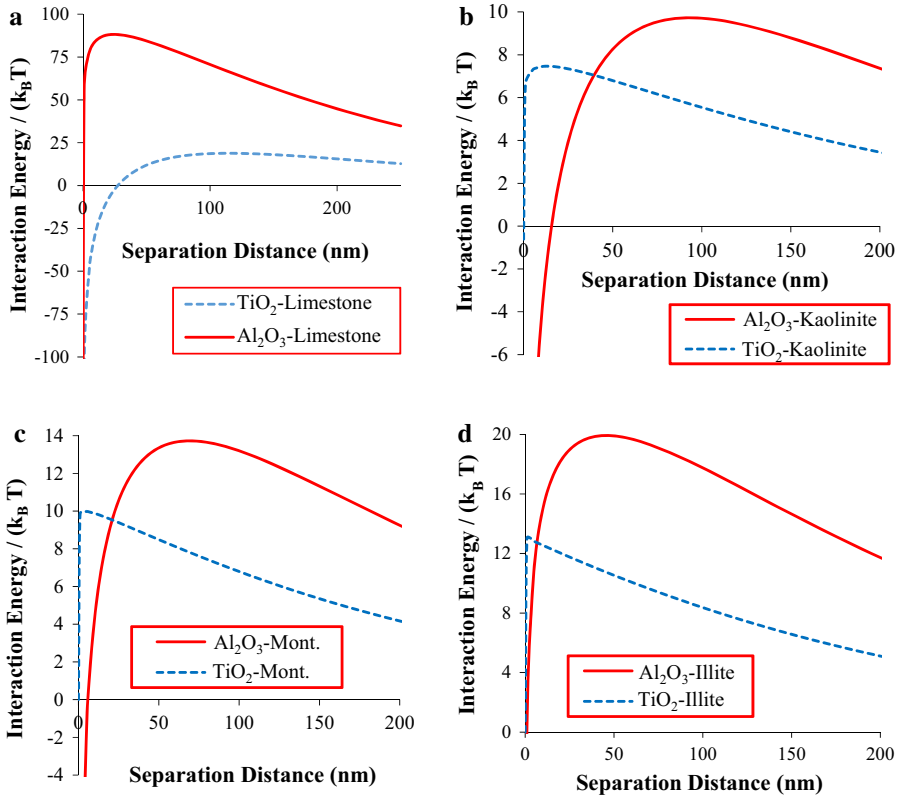

Fig. 4 DLVO calculations: Interaction energy curves versus separation distance between **a** the NPs and limestone grains, **b** the NPs and kaolinite particles, **c** the NPs and montmorillonite particles, **d** the NPs and illite particles

2011; Murphy 2012). However, it is worth pointing out that two recent studies found that the presence of suspended kaolinite particles noticeably increased TiO_2 and plutonium colloids mobilities through sandy porous media (Abdel-Fattah et al. 2013; Cai et al. 2014). It is believed that due to the intrinsic of engineered NPs and microbe properties, their stabilities in suspensions might be different. Thus, the distinct difference in the transport and aggregation of the NPs and bacteria (microbes) in the presence of kaolinite particles was observed.

To understand the reason(s) for the reduction of NPs recoveries in the presence of kaolinite, some factors were evaluated. For this purpose, the interaction force between the NPs and kaolinite particles was firstly determined by DLVO calculations. As shown in Fig. 4b, repulsion is a dominant force between the NPs and kaolinite particles. Thereby, retention of the NPs in the porous media was not due to the attraction between the NPs and the kaolinite particles. Caldelas (2010) and Murphy (2012) evaluated the effect of presence of kaolinite in sandy porous media on SiO_2-NPs transport. They found that presence of kaolinite in the porous media enlarged the specific surface area (SSA) of porous media which resulted in the available seats for NPs deposition to promote and consequently more SiO_2-NPs retained. To evaluate this reason, the *SSA* of the porous media with and without presence of kaolinite particles were measured using the BET surface area (A_{BET}) analyses. The results revealed that the SSA of porous media five and ten times increased in the presence of 2 and 4 vol % of kaolinite, respectively (Table 2). Although the results reveal that the NPs recoveries reduced with increasing the SSA of the porous media, we believe that this reason solely cannot be responsible for the reduction of NPs mobilities. Therefore, to complete this area of research, the location of kaolinite particles in the porous media should be investigated. Churcher and Dusseault (1991) proposed a model for location of clay particles in porous media. Based on this model, the clay particles locate within the pores and pore-throats, where the suspensions are supposed to pass, which results in the porous medium permeability reduction.

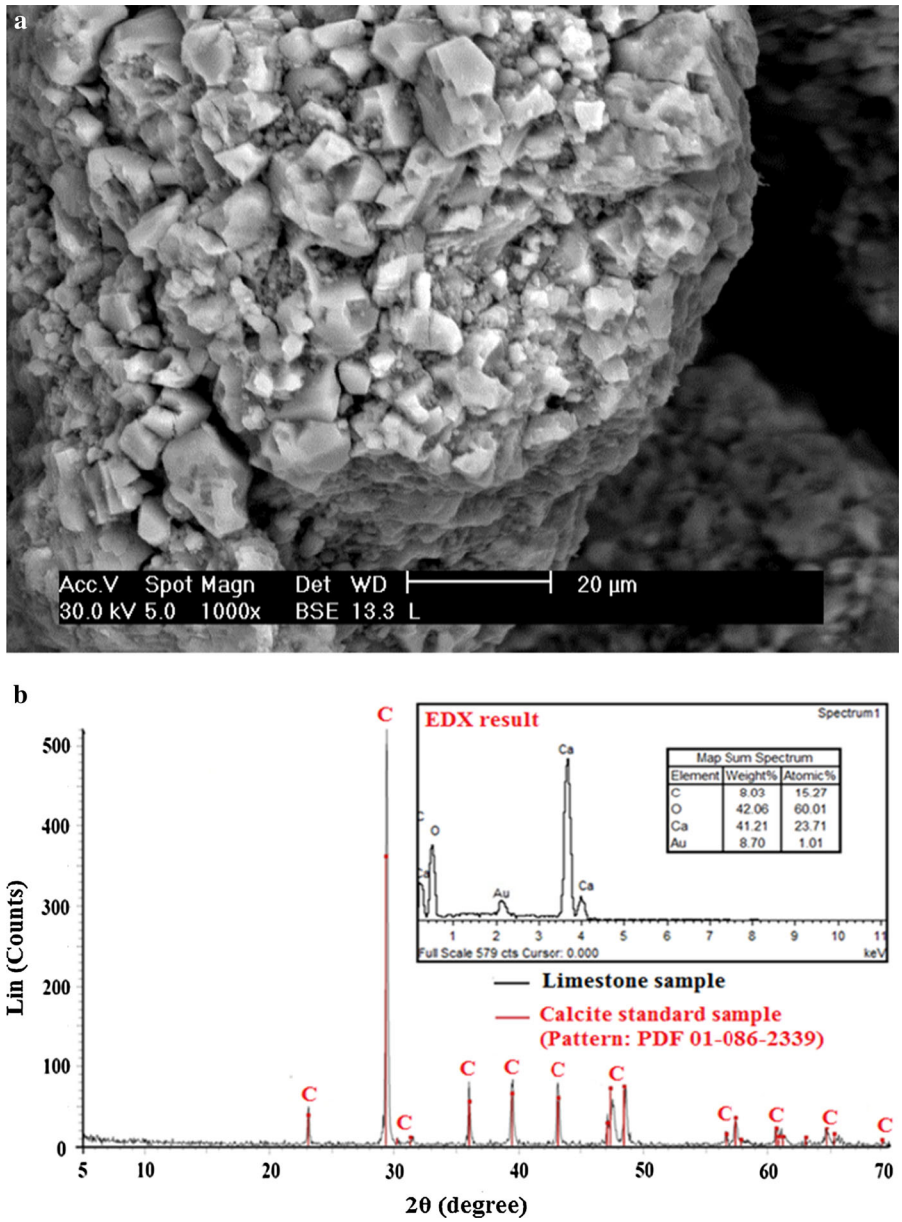

Fig. 5 **a** SEM image from a limestone grain, **b** XRD and EDX results from the limestone sample

As demonstrated in Table 1, the porous media permeabilities were considerably reduced with the increase in kaolinite concentration which confirms the kaolinite particles were located in the pore-throats. Now, with reference to the booklet shapes of kaolinite particles and their location in the pore-throats and pores, it can be concluded that when the NPs entered to the porous media, the NPs were trapped inside kaolinite particles. Thereby, the NPs recoveries were reduced in the presence of kaolinite. The NPs breakthrough curves obviously can also prove this hypothesis where the number of fluctuations (sinusoidal behavior) in NPs breakthrough curves (Fig. 3b) increases with the increase in kaolinite concentration which depicts that NPs could not elute continuously.

In addition, the FESEM and EDX analyses were carried out from the kaolinite particles after TiO_2-NPs transport through porous media to observe whether the NPs became trap inside the kaolinite particles. According to the XRD and EDX analyses

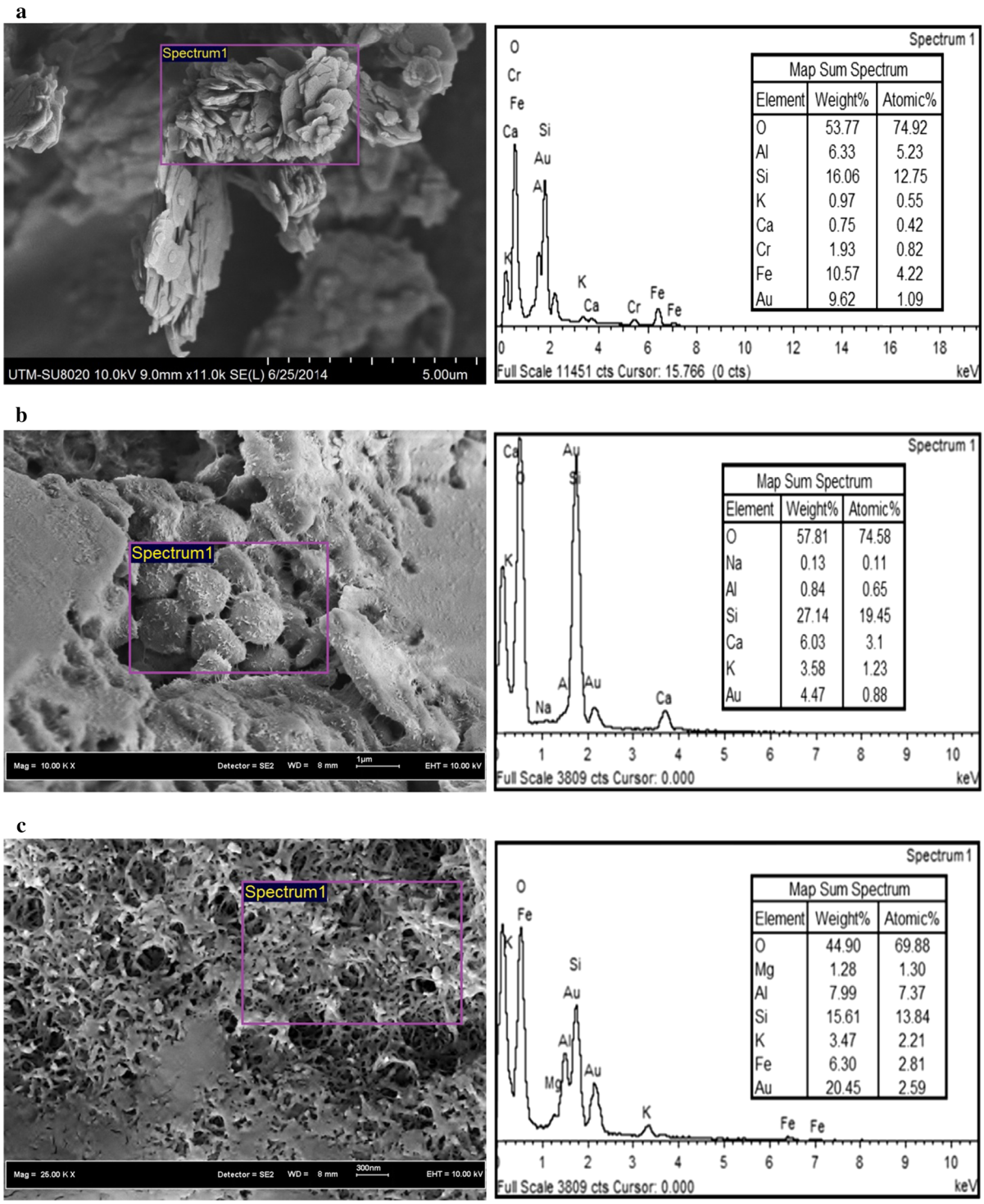

Fig. 6 FESEM (*right*) and EDX (*left*) analyses results from clay particles before the transportation tests **a** kaolinite, **b** montmorillonite, **c** illite

Table 1 Parameters for transportation of the NPs through limestone porous media in the presence different clay particles

NP type	Clay content	φ (%)	k (Darcy)	PV breakthrough	C/C_O (max)	No. of PVs	R_{NP} (%)
Al_2O_3	No clay	43	3.41	1.0	0.112	27.2	91.8
	2 vol% kaolinite	42	2.74	1.6	0.077	30.0	65.8
	4 vol% kaolinite	41	2.47	2.0	0.045	30.8	46.5
	2 vol% montmorillonite	40	2.61	1.6	0.064	30.6	60.4
	4 vol% montmorillonite	41	2.35	2.0	0.051	30.6	46.3
	2 vol% illite	42	2.50	2.0	0.062	31.2	55.7
	4 vol% illite	40	2.31	2.4	0.033	32.0	41.8
TiO_2	No clay	42	3.64	1.2	0.07	30.0	72.2
	2 vol% kaolinite	41	2.68	1.8	0.043	32.6	50.5
	4 vol% kaolinite	40	2.51	2.0	0.032	33.0	34.3
	2 vol% montmorillonite	41	2.70	1.8	0.039	33.0	47.3
	4 vol% montmorillonite	40	2.31	1.8	0.025	33.4	31.6
	2 vol% illite	44	2.43	2.0	0.036	32.8	41.3
	4 vol% illite	42	2.28	2.2	0.025	32.6	29.8

Table 2 BET measurements results

Sample	A_{BET} (m^2/gr)
Limestone	0.16
Kaolinite	10.91
Montmorillonite	131.86
Illite	95.41
Limestone + 2 vol% kaolinite	0.77
Limestone + 4 vol% kaolinite	1.36
Limestone + 2 vol% montmorillonite	2.9
Limestone + 4 vol% montmorillonite	5.63
Limestone + 2 vol% illite	2.27
Limestone + 4 vol% illite	4.37

from limestone grains and kaolinite particles before the transport tests (Figs. 5b, 6a), Ti was not detected as an element in them. However, as demonstrated in Fig. 7a, Ti was detected as an element beside of other kaolinite elements that confirms that TiO_2-NPs were trapped inside the kaolinite particles. It is believed that the same scenario was happened for Al_2O_3-NPs during transport through limestone in the presence of kaolinite.

Al_2O_3 and TiO_2 NPs transport in the presence of montmorillonite

The FESEM and EDX analyses results reveal that the morphology of montmorillonite particles is similar to cornflake and O, Si, Al, Na, Ca, and K are detected elements in this clay (Fig. 6b). Furthermore, the ζ-potential of montmorillonite was measured to be $+7.3 \pm 0.5$ mV.

The profiles of Al_2O_3 and TiO_2 NPs breakthrough curves are shown in Fig. 3c. The results depicted that the amounts of NPs recoveries declined to 60.4 and 46.3 % for the Al_2O_3-NPs and to 47.3 and 31.6 % for the TiO_2-NPs in the presence of 2 and 4 vol% of montmorillonite, respectively. The details of NPs transport tests in the presence of different montmorillonite concentrations are demonstrated in Table 1. Based on DLVO, the interaction forces between NPs and montmorillonite particles are repulsion (Fig. 4c). Thereby, the same reasons as explained for kaolinite are attributed for the NPs recovery reduction in the presence of montmorillonite. However, montmorillonite as compared to kaolinite caused more quantities of the NPs to be retained in the porous media. The larger *SSA* in the presence of montmorillonite is one of the reasons which provide more seats for the NPs retention (Table 2). Furthermore, the permeability coefficients of porous media in the presence of montmorillonite were lower than kaolinite, that reveal that the montmorillonite particles occupied more spaces in the pores (Table 1). Therefore, the chance of mutual interaction between the NPs and montmorillonite particles promoted which have caused more NPs to be trapped inside the montmorillonite particles. The FESEM and EDX analyses from montmorillonite

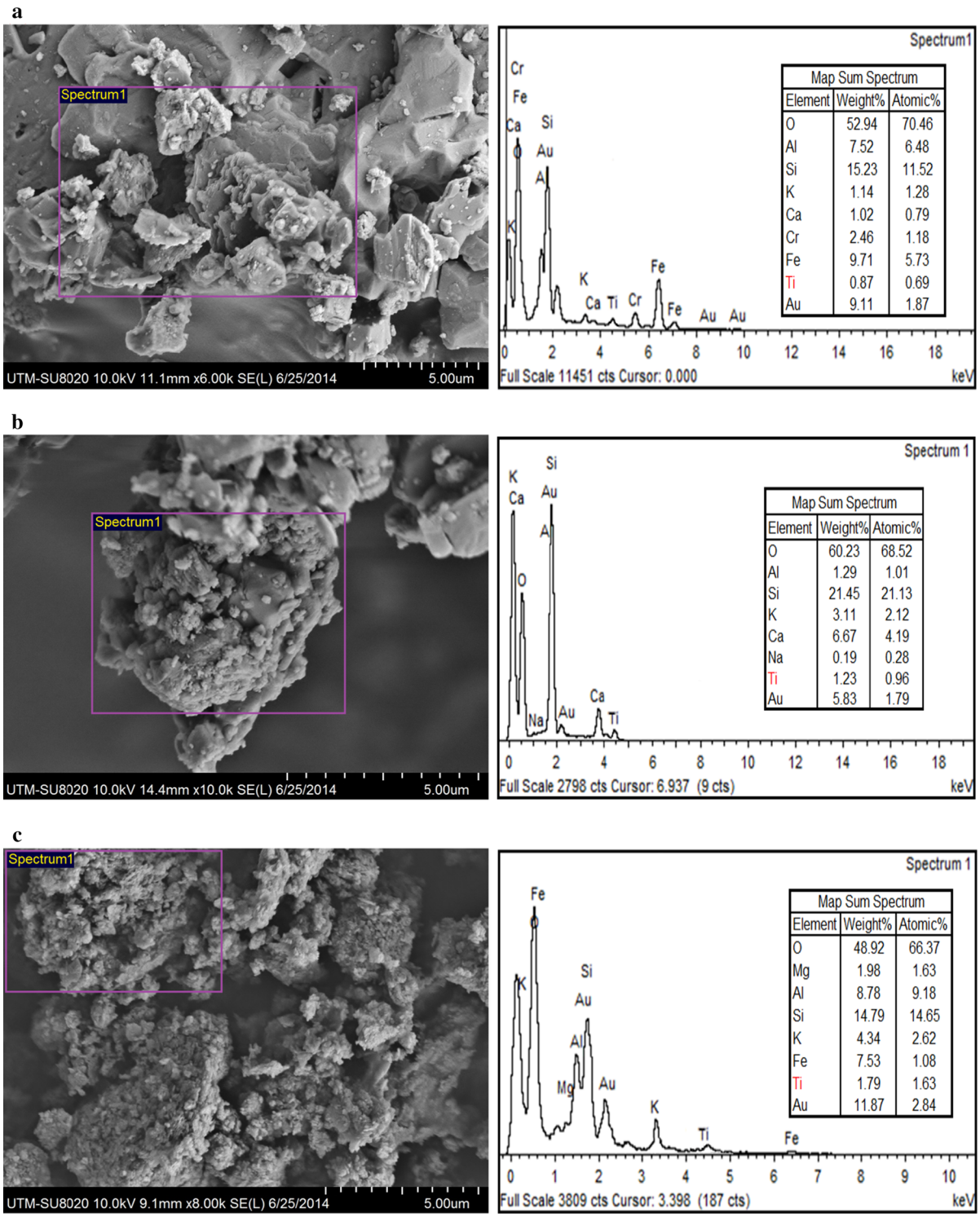

Fig. 7 FESEM (*right*) and EDX (*left*) analyses results from clay particles after the TiO_2-NPs transportation tests **a** kaolinite, **b** montmorillonite, **c** illite

particles after TiO_2-NPs transport demonstrated that TiO_2-NPs were trapped inside the montmorillonite particles (Fig. 7b).

Al_2O_3 and TiO_2 NPs transport in the presence of illite

As shown in Fig. 6c, the morphology of illite particles is fibrous and the elements including O, Si, Al, Mg, K, and Fe are also detected in this sample. The ζ-potential of illite was also measured to be $+8.9 \pm 0.5$ mV. The NPs transport tests results in the presence of 2 and 4 vol% of illite particles revealed that the amounts of NPs recoveries reduced to 55.7 and 41.8 %, respectively for the Al_2O_3-NPs and to 41.3 and 29.8 %, respectively for the TiO_2-NPs. The profiles of Al_2O_3 and TiO_2 NPs breakthrough curves in the presence of illite particles are shown in Fig. 3d. For further information on NPs transport tests in the presence of illite particles refer to Table 1. Since the interaction force between the NPs and illite particles is repulsive (Fig. 4d), the same reasons as the two previous clay particles are allocated for the NPs retention. The FESEM and EDX analyses from illite particles after TiO_2-NPs transport also confirmed that TiO_2-NPs were trapped inside the illite particles (Fig. 7c). However, illite in comparison to montmorillonite and kaolinite is more effective for NPs retention in porous media. The porous media characterizations in the presence of illite demonstrated that the permeability coefficients of porous media had higher reduction as compared to two previous clays which depicts illite particles occupied more spaces in pores. Moreover, the fibrous structure of illite provides more spaces for the NPs retention.

Conclusion

The outcomes from this study have provided some insights on the influence of abundant clay particles including kaolinite, montmorillonite, and illite in the limestone porous medium on the transport and retention of Al_2O_3 and TiO_2 NPs. The interactions of NPs with clay particles are very plausible due to the position of clay particles which are mostly located in the pore-throats, and consequently expected to influence the fate of NPs in porous media. It was found that Al_2O_3 and TiO_2 NPs recoveries had noticeably declined as a result of the presence of these clays in the porous media. The main reasons are attributed to the position of clay particles in pore-throats and morphology of the clays which caused the NPs to become trapped inside them. The results also revealed that the presence of illite in the porous medium had caused more NPs to be retained in comparison to montmorillonite and kaolinite. Although the experimental tests were carried out on small-scale columns and in only one type of porous medium, the aforementioned outcomes remarkably revealed that the mobility of Al_2O_3 and TiO_2 NPs through porous media is very sensitive to the type and concentration of clay particles.

Acknowledgments The authors gratefully acknowledge Universiti Teknologi Malaysia (UTM) which provided materials and equipment. Research support was also provided by the UTM grant No. Q.J130000.2542.06H82 and R.J30000.7842.4F562.

References

Abdel-Fattah AI, Zhou D, Boukhalfa H, Tarimala S, Ware SD, Keller AA (2013) Dispersion stability and electrokinetic properties of intrinsic plutonium colloids: implications for subsurface transport. Environ Sci Technol 47(11):5626–5634

Aiken GR, Hsu-Kim H, Ryan JN (2011) Influence of dissolved organic matter on the environmental fate of metals, nanoparticles, and colloids. Environ Sci Technol 45(8): 3196–3201

Auffan M, Rose J, Bottero JY, Lowry GV, Jolivet JP, Wiesner MR (2009) Towards a definition of inorganic nanoparticles from an environmental, health and safety perspective. Nat Nano 4(10):634–641

Ben-Moshe T, Dror B, Berkowitz I (2010) Transport of metal oxide nanoparticles in saturated porous media. Chemosphere 81(3):387–393

Bian SW, Mudunkotuwa IA, Rupasinghe T, Grassian VH (2011) Aggregation and dissolution of 4 nm ZnO nanoparticles in aqueous environments: influence of pH, ionic strength, size, and adsorption of humic acid. Langmuir 27(10):6059–6068

Cai L, Tong M, Wang X, Kim H (2014) Influence of clay particles on the transport and retention of titanium dioxide nanoparticles in quartz sand. Environ Sci Technol 48(13): 7323–7332

Caldelas FM (2010) Experimental parameter analysis of nanoparticle retention in porous media. Master Thesis, University of Texas at Austin

Chen G, Liu X, Su C (2011) Transport and retention of TiO_2 rutile nanoparticles in saturated porous media under low ionic- strength conditions: measurements and mechanisms. Langmuir 27(9):5393–5402

Chowdhury I, Hong Y, Honda RJ, Walker SL (2011) Mechanisms of TiO_2 nanoparticle transport in porous media: role of solution chemistry, nanoparticle concentration, and flowrate. J Colloid Interface Sci 360(2):548–555

Churcher PL, Dusseault B, Survey OG (1991) Clay distribution in carbonate reservoirs: examples from the silurian of Southwestern Ontario. Ontario Ministry of Northern Development and Mines, Ontario Geological Survey

Darlington TK, Neigh AM, Spencer MT, Nguyen OT, Oldenburg SJ (2009) Nanoparticle characteristics affecting environmental fate and transport through soil. Environ Toxicol Chem 28(6):1191–1199

Esfandyari Bayat A, Junin R, Derahman MN, Samad AA (2015) TiO_2 nanoparticle transport and retention through saturated limestone porous media under various ionic strength conditions. Chemosphere 134:7-15. doi:10.1016/j.chemosphere.2015.03.052

Esfandyari Bayat A, Junin R, Ghadikolaei FD, Piroozian A (2014a) Transport and aggregation of Al_2O_3 nanoparticles through saturated limestone under high ionic strength conditions: measurements and mechanisms. J Nanopart Res 16(12):1–12

Esfandyari Bayat A, Junin R, Samsuri A, Piroozian A, Hokmabadi M (2014b) Impact of metal oxide nanoparticles on enhanced oil recovery from limestone media at several temperatures. Energy Fuels 28(10):6255–6266

Fang J, Shan XQ, Wen B, Lin JM, Owens G (2009) Stability of titania nanoparticles in soil suspensions and transport in saturated homogeneous soil columns. Environ Pollut 157(4):1101–1109

French RA, Jacobson AR, Kim B, Isley SL, Penn RL, Baveye PC (2009) Influence of ionic strength, pH, and cation valence on aggregation kinetics of titanium dioxide nanoparticles. Environ Sci Technol 43(5):1354–1359

Godinez IG, Darnault CJG (2011) Aggregation and transport of nano-TiO_2 in saturated porous media: effects of pH, surfactants and flow velocity. Water Res 45(2):839–851

Handy RD, Shaw BJ (2007) Toxic effects of nanoparticles and nanomaterials: implications for public health, risk assessment and the public perception of nanotechnology. Health Risk Soc 9(2):125–144

Hendraningrat L, Torsæter O (2015) Metal oxide-based nanoparticles: revealing their potential to enhance oil recovery in different wettability systems. Appl Nanosci 5(2):181–199

Hotze EM, Phenrat T, Lowry GV (2010) Nanoparticle Aggregation: challenges to understanding transport and reactivity in the environment. J Environ Qual 39(6):1909–1924

Jiang J, Oberdörster G, Biswas P (2009) Characterization of size, surface charge, and agglomeration state of nanoparticle dispersions for toxicological studies. J Nanopart Res 11(1):77–89

Jiang S (2012) Clay minerals from the perspective of oil and gas exploration, clay minerals in nature—their characterization. Modification and Application. InTech. doi:10.5772/47790

Jiang X, Tong M, Lu R, Kim H (2012) Transport and deposition of ZnO nanoparticles in saturated porous media. Colloids Surf A 401:29–37

Krewski D, Yokel RA, Nieboer E, Borchelt D, Cohen J, Harry J, Kacew S, Lindsay J, Mahfouz AM, Rondeau V (2007) Human health risk assessment for aluminum, aluminum oxide and aluminum hydroxide. J Toxicol Environ Health B Crit Rev 10(1):1–269

Lecoanet HF, Bottero JY, Wiesner MR (2004) Laboratory assessment of the mobility of nanomaterials in porous media. Environ Sci Technol 38(19):5164–5169

Murphy MJ (2012). Experimental analysis of electrostatic and hydrodynamic forces affecting nanoparticle retention in porous media. Master Thesis, University of Texas at Austin

Nel A, Xia T, Mädler L, Li N (2006) Toxic potential of materials at the nanolevel. Science 311(5761):622–627

Petosa AR, Jaisi DP, Quevedo IR, Elimelech M, Tufenkji N (2010) Aggregation and deposition of engineered nanomaterials in aquatic environments: role of physicochemical interactions. Environ Sci Technol 44(17):6532–6549

Phenrat T, Saleh N, Sirk K, Kim HJ, Tilton R, Lowry G (2008) Stabilization of aqueous nanoscale zerovalent iron dispersions by anionic polyelectrolytes: adsorbed anionic polyelectrolyte layer properties and their effect on aggregation and sedimentation. J Nanopart Res 10(5):795–814

Piccinno F, Gottschalk F, Seeger S, Nowack B (2012) Industrial production quantities and uses of ten engineered nanomaterials in Europe and the world. J Nanopart Res 14(9):1–11

Salehi M, Johnson SJ, Liang JT (2008) Mechanistic study of wettability alteration using surfactants with applications in naturally fractured reservoirs. Langmuir 24(24):14099–14107

Schroth BK, Sposito G (1997) Surface charge properties of kaolinite. Clays Clay Miner 45:85–91

Scown TM, Van Aerle R, Tyler CR (2010) Review: do engineered nanoparticles pose a significant threat to the aquatic environment? Crit Rev Toxicol 40(7):653–670

Syngouna VI, Chrysikopoulos CV (2013) Cotransport of clay colloids and viruses in water saturated porous media. Colloids Surf A 416:56–65

Tufenkji N, Elimelech M (2004) Deviation from the classical colloid filtration theory in the presence of repulsive DLVO interactions. Langmuir 20(25):10818–10828

Vasiliadou IA, Chrysikopoulos CV (2011) Cotransport of Pseudomonas putida and kaolinite particles through water-saturated columns packed with glass beads. Water Resour Res 47(2):W02543

Wang C, Wei J, Xia B, Chen X, He B (2013) Effect of nano-silica on the mechanical, thermal, and crystalline properties of poly (vinyl alcohol)/nano-silica films. J Appl Polym Sci 128(3):1652–1658

Wilson MJ, Wilson L, Patey I (2014) The influence of individual clay minerals on formation damage of reservoir sandstones: a critical review with some new insights. Clay Miner 49(2):147–164

Yang H, Tong M, Kim H (2012) Influence of bentonite particles on representative gram negative and gram positive bacterial deposition in porous media. Environ Sci Technol 46(21):11627–11634

Yu J, An C, Mo D, Liu N, Lee RL (2012) Study of adsorption and transportation behavior of nanoparticles in three different porous media. SPE improved oil recovery symposium, Tulsa, 14–18 April. doi:10.2118/153337-MS